Soil Dynamics and Earthquake Engineering 208 (2026) 110411

Contents lists available at ScienceDirect

Soil Dynamics and Earthquake Engineering

journal homepage: www.elsevier.com/locate/soildyn

Lateral kinematic response of single-pile bridge pier foundations under seismic waves: Linear versus non-linear soil behaviour

Eduardo Rodríguez-Galván [a,*], Sandro Carbonari [b], Francesca Dezi [c], Guillermo M. Álamo [a], Juan J. Aznárez [a], Orlando Maeso [a], Graziano Leoni [d]

[a] University Institute of Intelligent Systems and Numerical Applications in Engineering (SIANI), Universidad de Las Palmas de Gran Canaria, 35017, Las Palmas de Gran Canaria, Spain
[b] Department of Construction, Civil Engineering and Architecture (DICEA), Università Politecnica delle Marche, 60131, Ancona, Italy
[c] Geology Division, School of Science and Technology, University of Camerino, 62032, Camerino, Italy
[d] School of Architecture and Design (SAAD), University of Camerino, 63100, Camerino, Italy

ARTICLE INFO

Keywords:
Pile foundation
Soil–structure interaction
Kinematic interaction
Non-linear analysis
Seismic analysis
Site response
BDWF model

ABSTRACT

This paper analyses the kinematic response of single-pile bridge foundations subjected to vertically propagating seismic S-waves, considering both linear and non-linear soil behaviours. Two one-dimensional soil models are adopted to compute the free-field responses: (i) the conventional elastic propagation model for layered soils, and (ii) a non-linear lumped-parameter formulation incorporating the modified Kondner and Zelasko shear stress–strain relationship and extended Masing rules. Different Beam on Dynamic Winkler Foundation (BDWF) formulations are examined to model soil–pile interaction, including linear formulations proposed by Gazetas and Dobry, and non-linear expressions proposed by recommended practices. The degradation of soil stiffness derived from the non-linear soil site response is also incorporated into selected BDWF formulations. The seismic response of floating and end-bearing piles embedded in both homogeneous and non-homogeneous sandy soils, characterised by different stiffness levels, is considered. The soil–pile seismic response is analysed in terms of mean envelopes of bending moments and shear forces obtained from ten earthquakes. Results show that the soil behaviour under S-wave propagation considerably affects the free-field soil response, and consequently, the pile kinematic response. Overall, both non-linear soil models and BDWF formulations generally lead to greater internal forces, while neglecting soil stiffness degradation within the soil–pile interaction modelling proves to be a conservative assumption. The findings provide insight into the importance of modelling assumptions, offering guidance for selecting analysis strategies in the seismic assessment of deep foundations, particularly when site-specific data are unavailable and rigorous numerical models are not feasible, such as in parametric studies or preliminary design stages.

1. Introduction

Deep foundations such as piles are widely adopted in geotechnical engineering to ensure adequate bearing capacity and deformation control when surface soils are soft, heterogeneous, or otherwise unsuitable for shallow foundations. These features have led to their widespread application in various types of structures, such as buildings, bridges and offshore platforms [1,2].

In bridge engineering, piles play a crucial role, particularly when structures are built over riverbeds, soft soils, or in seismically active regions. Under these conditions, foundations must withstand substantial axial loads as well as a wide range of lateral forces induced by wind, water flows, ground shaking or soil deformations. Under these conditions, soil–structure interaction (SSI) plays a pivotal role in controlling the system's seismic response. Neglecting SSI may lead to unconservative or overly conservative predictions, depending on the soil–foundation–structure configuration, the characteristics of the applied loading, and how these interact with the properties of the SSI system, as it has been discussed in [3]. Properly accounting for SSI is thus a fundamental requirement for reliable seismic design and performance assessment of bridge foundations.

Several rigorous numerical models have been developed to reproduce the coupled dynamic behaviour of SSI [4–8], most of them based on the finite element method, often supplemented by boundary

* Corresponding author.
E-mail addresses: eduardo.rodriguezgalvan@ulpgc.es (E. Rodríguez-Galván), s.carbonari@staff.univpm.it (S. Carbonari), francesca.dezi@unicam.it (F. Dezi), guillermo.alamo@ulpgc.es (G.M. Álamo), juanjose.aznarez@ulpgc.es (J.J. Aznárez), orlando.maeso@ulpgc.es (O. Maeso), graziano.leoni@unicam.it (G. Leoni).

https://doi.org/10.1016/j.soildyn.2026.110411
Received 15 January 2026; Received in revised form 16 May 2026; Accepted 19 May 2026
Available online 28 May 2026

element formulations to account for far-field wave propagation and radiation. While these approaches allow detailed modelling of both linear and non-linear soil behaviour, their high computational cost limits their applicability for extensive parametric studies or routine engineering practice. For this reason, simplified SSI models have been developed for both linear and non-linear behaviours. Linear or quasi-linear interaction models assume a proportional load–displacement relationship. The substructure method is typically employed where SSI behaviour is reproduced through frequency dependent impedance functions and kinematic interaction factors [9–11], or through lumped parameter models [12–14]. Linear SSI can also be modelled using Beam on Dynamic Winkler Foundation (BDWF) formulations, where depth-distributed impedance functions that incorporate stiffness and radiation damping in a frequency-dependent manner are adopted [15,16]. Linear assumptions offer efficiency and practicality but cannot reproduce the soil's cyclic degradation under strong shaking. To overcome this limitation, non-linear approaches based on p–y curves are widely used in performance-based design [17,18]. Additionally, non-linear models can simulate cyclic loading effects through appropriate loading–unloading rules, thereby capturing the hysteretic response of the system, and generally provide a more realistic representation of soil–pile interaction, although at a higher computational cost due to the iterative solution procedures.

During earthquake events, the lateral loads acting on piles arise from two main sources: the inertial forces transmitted from the superstructure (inertial interaction), and kinematic loads generated by soil deformations induced by the wave propagation. The latter kinematic interaction is particularly relevant for long slender piles embedded in stiff-over-soft deposits or stratigraphic profiles with strong impedance contrasts, where soil curvature can induce significant bending even in the absence of inertial effects, as reported in the review conducted by Di Laora and Rovithis [19]. Several studies have addressed kinematic pile response under vertical S-wave propagation [15,20–28]. For instance, Anoyatis et al. [25] analysed various tip and head boundary conditions in kinematic soil–pile interaction excited by vertically propagating harmonic S-waves, using a linear BDWF model and assuming a homogeneous soil layer. Their aim was to derive analytical and closed-form solutions for pile response. Stacul et al. [27] examined kinematic pile-head bending moments and foundation input motions under increasing earthquake-induced shear strains. They employed a one-dimensional model to capture the non-linear free-field soil response and a detailed 3D finite difference model to reproduce the full SSI system. These analyses were conducted to develop an equivalent-linear procedure suitable for practical engineering applications, offering an effective alternative for modelling soil–pile interaction, even when the free-field soil response exhibits marked non-linearity. Di Laora and Rovithis [28] investigated kinematic pile-head bending in inhomogeneous soils by applying a linear BDWF formulation subjected to harmonic S-waves, proposing design expressions for estimating kinematic pile-head moments.

Despite the extensive literature on the subject, most studies rely on either linear or non-linear assumptions for seismic wave propagation in the soil and for the soil–pile interaction model itself, without clearly distinguishing between the different sources of non-linearity. As a result, the effects of soil non-linearity on the kinematic response remain difficult to interpret in a systematic way, particularly when different modelling assumptions are combined. This gap is significant because soil non-linearity affects the kinematic response through two concurrent mechanisms: (i) modification of the free-field motion due to stiffness degradation and hysteretic damping during wave propagation; (ii) variation of the soil–pile reaction forces, governed by non-linear behaviour and strain-dependent soil stiffness. However, a systematic and coupled assessment of these two mechanisms is still largely missing in the literature. For these reasons, the main objective of this study is to provide a consistent framework in which these two sources of non-linearity can be analysed both independently and in combination. Thus, the proposed paper aims to improve the understanding of how different approaches to modelling soil non-linearity (in wave propagation, soil–pile interaction models, or both) affect the predicted kinematic demand on single-piles bridge pier foundations. This approach allows the specific role of each non-linear modelling component to be identified, not only in terms of response amplitude but also in terms of the depth-dependent distribution of soil deformation. To this end, two one-dimensional soil modelling approaches are assessed for evaluating the free-field response (FFR): (i) the classical analytical solution for vertical S-wave in layered elastic media, and (ii) a lumped parameter model [29] capable of reproducing non-linear stress–strain behaviour through the modified Kondner–Zelasko formulation [30,31]. The FFRs obtained from these models are combined with several BDWF formulations, ranging from linear Winkler-type expressions [32] to non-linear $p-y$ curves recommended by API guidelines [18]. All these models have been specifically tailored to isolate non-linear effects, enabling a systematic analysis of their influence. Additionally, the stiffness degradation derived from the non-linear soil behaviour under vertical S-wave propagation is introduced in the BDWF models. The analysis is carried out for a representative range of conditions, with the aim of identifying how these non-linear mechanisms influence not only the magnitude of the response but also the shape of the free-field displacement profile, which directly controls the curvature demand and, consequently, the kinematic bending in piles under seismic loading. The findings also support the identification of appropriate modelling strategies for capturing kinematic effects in single-pile bridge foundations, thereby advancing the design and seismic analysis of these systems.

The remainder of the paper is organised as follows: Section 2 outlines the soil and BDWF modelling approaches; Section 3 describes the analysed configurations and seismic excitations; Section 4 discusses the results; and Section 5 summarises the main findings and implications for engineering practice.

2. Methodology

2.1. Soil models

The FFR for the linear elastic soil is determined by the classical harmonic one-dimensional S-wave propagation problem, depicted in Fig. 1. The problem is formulated in the frequency domain considering the upward propagation of unit amplitude S-waves from a bedrock (u_{ff}, see Fig. 1) underlying a horizontally layered soil deposit discretised into N horizontal layers, each characterised by thickness (h_j), shear modulus (G_j), and wavenumber (q_j):

$$q_j = \frac{\omega}{V_{sj}} \tag{1}$$

being ω the angular frequency, and V_{sj} the shear wave velocity of layer j. The resulting horizontal displacements in each layer produced by the incident field are determined by solving the governing shear wave equation in an elastic medium:

$$\frac{\partial^2 u_j(z)}{\partial t^2} = V_{sj}^2 \frac{\partial^2 u_j(z)}{\partial z^2}, \qquad z \in [z_{j-1}, z_j] \tag{2}$$

where t is the time, and z the depth measured from ground surface. Assuming harmonic motion ($u_j(z,t) = u_j(z)e^{-i\omega t}$), the general solution of Eq. (2) is:

$$u_j(z) = A_j e^{-iq_j z} + B_j e^{iq_j z}, \quad z \in [z_{j-1}, z_j] \tag{3}$$

being A_j and B_j the amplitudes of incident and reflected waves. Continuity conditions are expressed at the interface of adjacent layers (j and $j+1$) in terms of displacement and shear stress according to:

$$u_j(z_j) = u_{j+1}(z_j) \tag{4}$$

$$\tau_j(z_j) = \tau_{j+1}(z_j) \tag{5}$$

where the shear stress of the jth layer can be determined as follows:

$$\tau_j(z) = G_j \frac{\partial u_j}{\partial z} = G_j(-\mathrm{i}q_j A_j \mathrm{e}^{-\mathrm{i}q_j z} + \mathrm{i}q_j B_j \mathrm{e}^{\mathrm{i}q_j z}) \tag{6}$$

Boundary conditions are formulated at the bedrock level, where the motion is imposed ($u_N(z_N) = 1$), and at the free surface, where shear stress is null ($\tau_1(0) = 0$). Eqs. (4)–(6) lead to a system of $2N$ equations for the $2N$ unknowns of the system (A_j and B_j). Once the wave amplitudes of each layer (A_j and B_j) have been determined, the displacement at any desired depth (z) is computed following Eq. (3). Afterwards, velocities and accelerations are obtained via:

$$v(z) = \mathrm{i}\omega u(z) \tag{7}$$

$$a(z) = -\omega^2 u(z) \tag{8}$$

In view of the problem linearity, above expressions can be regarded as Frequency Response Functions (FRFs), which provide the soil FFR starting from the known motion at the bedrock. The latter can be computed applying the Fourier transform to the acceleration time history recorded at the bedrock level. Finally, the kinematic response quantities can be expressed in the time domain, through the inverse Fourier transform (see, e.g., [33]).

The non-linear behaviour of soil under vertical S-wave propagation is simulated through a lumped-parameter model capable of reproducing soil stiffness degradation and hysteretic damping. Each soil layer is represented by a mass, a non-linear spring, and a viscous damper (Fig. 2). The non-linear backbone shear stress–strain curve follows the modified Kondner–Zelasko relationship [30,31]:

$$\tau_{bb}(\gamma) = \frac{G_0 \gamma}{1 + \beta\left(\frac{\gamma}{\gamma_R}\right)^s} \tag{9}$$

where τ, γ and G_0, are the shear stress, strain, and initial (maximum or non-degraded) shear modulus, respectively; γ_R is the reference shear strain parameter; and β and s are two dimensionless shape parameters. Above parameters are obtained through fitting the normalised shear modulus and damping curves. Confining-stress dependency is incorporated through the relationship proposed by Hashash and Park [29]:

$$\gamma_R = \gamma_{Ref} \left(\frac{\sigma'_v}{\sigma'_{Ref}}\right)^b \tag{10}$$

being σ'_v the effective vertical stress, σ'_{Ref} the reference effective vertical stress at which $\gamma_{Ref} = \gamma_R$, and b is a model parameter. For the jth layer, the tributary mass (m_j) is determined as follows:

$$m_j = \rho_j h_j \tag{11}$$

being ρ_j and h_j the density and thickness of layer j. To construct the soil mass matrix ($\mathbf{M_s}$), half of the mass from each adjacent layer is lumped together at their shared boundary (see Fig. 2). The stiffness of the jth layer (k_j) can be calculated at each time instant as:

$$k_j = \frac{G_j}{h_j} = \frac{1}{h_j} \frac{\mathrm{d}\tau_j(\gamma_j)}{\mathrm{d}\gamma_j} \tag{12}$$

At each time step, the shear modulus value is updated based on the derivative of $\tau_j(\gamma_j)$ with respect to γ_j. Once the stiffness of each layer has been determined, the stiffness soil matrix ($\mathbf{K_s}$) is formed, updating it at each time step to reflect the non-linear soil behaviour.

The cyclic soil behaviour is simulated through the extended Masing rules (see, e.g., [34] and Fig. 3), commonly used for accurately capturing the energy dissipation and non-linear hysteretic behaviour of soils undergoing cyclic loading. For the sake of completeness, the hysteretic rules are reported below:

- The stress–strain response follows the backbone curve (Eq. (9)) during initial loading (from point A to B in Fig. 3).
- If a stress reversal is given at any point (τ_r, γ_r) (e.g., point B of Fig. 3), the stress–strain trajectory subsequently follows a path determined by:

$$\frac{\tau - \tau_r}{2} = \tau_{bb}\left(\frac{\gamma - \gamma_r}{2}\right) \tag{13}$$

- If the unloading or reloading response exceeds the previous maximum strain and intersects the backbone curve, the path follows the backbone curve until the next stress reversal (from C to D in Fig. 3).
- If an unloading or reloading curve from the previous cycle is crossed, the stress–strain path follows that of the previous cycle (from G to F in Fig. 3).

Soil non-linearity and cyclic rules intrinsically account for the soil hysteretic damping at medium-high strains. However, as the stress–strain response is nearly linear at very small strains (hysteretic damping is close to zero), it is necessary to consider small strain damping to avoid numerical problems and to provide a reliable modelling of the soil response at small strains. The small strain viscous damping is incorporated using the Rayleigh formulation, which allows formulating the following damping matrix $\mathbf{C_s}$ (see, e.g., [33]):

$$\mathbf{C_s} = A\mathbf{M_s} + B\mathbf{K_s} \tag{14}$$

where $\mathbf{M_s}$ and $\mathbf{K_s}$ are the soil mass and stiffness matrices. Parameters A and B are computed as:

$$A = \zeta \frac{2\omega_c \omega_d}{\omega_c + \omega_d} \tag{15}$$

$$B = \zeta \frac{2}{\omega_c + \omega_d} \tag{16}$$

being ω_c and ω_d the natural frequencies of the cth and dth soil modes, and ζ the damping ratio for these two modes. In this work, a soil damping ratio of 2.5% is adopted, and the fundamental mode and the first mode with a frequency exceeding five times that of the fundamental are considered, following recommendation by Kwok et al. [35] in order to simulate an overall damping not exceeding ζ for a significant number of vibration modes contributing to the soil response. The initial stiffness is used to assemble the soil damping matrix; this assumption is typically adopted because it has been demonstrated that similar results are obtained using initial and tangent stiffness matrices if the soil undergoes significant non-linearities so that the main damping is due to the hysteretic behaviour (see, e.g., [36]). In addition, a viscous dashpot (C_B) is added at the degree of freedom corresponding to the bedrock, in order to reproduce the radiation condition (see Fig. 2):

$$C_B = \rho_B V_{sB} \tag{17}$$

where ρ_B and V_{sB} are the density and shear wave velocity of the bedrock.

The displacements, velocities, and accelerations of the non-linear soil are computed by solving the dynamic governing equation in time domain:

$$\mathbf{M_s}\ddot{\vec{u}}_s(t) + \mathbf{C_s}\dot{\vec{u}}_s(t) + \mathbf{K_s}(t)\vec{u}_s(t) = \vec{f}_s(t) \tag{18}$$

where $\ddot{\vec{u}}_s$, $\dot{\vec{u}}_s$ and $\vec{u}_s$ are the vectors of nodal accelerations, velocities, and displacements of the soil, respectively; and $\vec{f}_s$ is the nodal force vector, which is composed by the excitation force located at the bedrock level, representing a viscous force per unit area that is expressed as:

$$\vec{f}_B(t) = C_B \dot{\vec{u}}_B(t) \tag{19}$$

being $\dot{\vec{u}}_B(t)$ the velocity vector at the bedrock, corresponding to the velocities of the incoming seismic signal. It is important to note that, in this non-linear soil model, the bedrock moves according to the imposed seismic motion (see Fig. 2) in absence of the soil column, while it can experience different motion as a consequence of waves propagating on

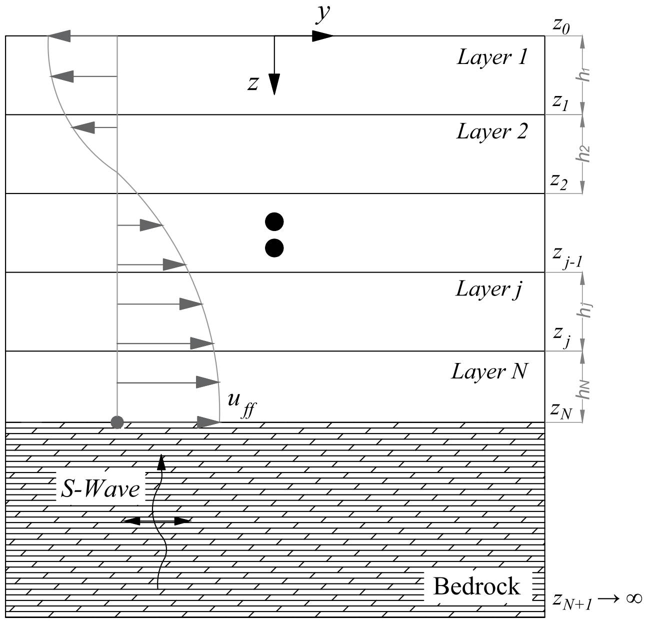

Fig. 1. One-dimensional linear soil model under vertical S-wave propagation.

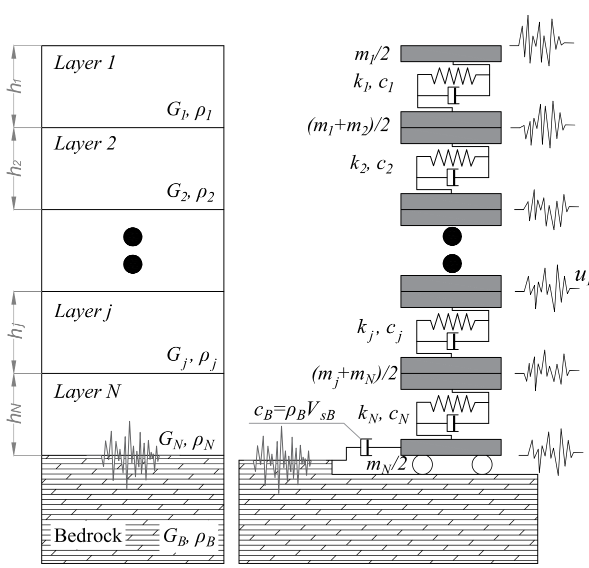

Fig. 2. One-dimensional non-linear soil model under vertical S-wave propagation.
Source: Adapted from [29]

the outgoing direction; this allows simulating the radiation condition at the bedrock level avoiding artificial amplification.

The iterative Newmark method for non-linear systems (see, e.g., [33]) is employed to integrate Eq. (18), by using the average acceleration method. In order to ensure that the final solution is sufficiently accurate, the following convergence criterion is established in terms of the shear strain differences obtained in each layer between two consecutive iterations:

$$|\Delta\vec{\gamma}_s| \leq 10^{-12} \tag{20}$$

In order to preserve the continuity of the main content of this work, the validation of this one-dimensional non-linear soil model against DeepSoil [37] is provided in Appendix.

2.2. Pile and soil–structure interaction modelling

The seismic response of the soil–pile system is obtained through the BDWF approach, by modelling the pile with finite elements and adopting linear and non-linear models to reproduce the soil–pile interaction forces (see Fig. 4). In detail, the pile is modelled using Euler–Bernoulli beam finite elements, where each node has two degrees of freedom: lateral and rotational motions. The axial behaviour, being decoupled from the flexural one for the Euler–Bernoulli beam, is not modelled because it does not affect the lateral seismic behaviour of the single pile, which is the objective of this work. The material damping is accounted for through the Rayleigh approach, calibrating coefficients in order to have a 2% damping ratio in correspondence of the pile's (without soil–pile interaction) fundamental mode, and the first one that exceeds five times the fundamental frequency. This choice ensures selecting two separated frequencies, so that the damping ratio is correctly reproduced in the modal range governing the response, without introducing excessive artificial damping at high frequencies. No soil–pile interaction is considered for determining the pile modes in the computation of the Rayleigh damping. In this way, the same Rayleigh damping is applied independently of the SSI typology, and no additional damping is introduced when the SSI model already includes hysteretic behaviour.

Following the BDWF approach, the soil–pile interaction is represented by discrete Winkler springs and radiation dashpots distributed along the pile depth. Four BDWF variants are examined in this work, each one incorporating different soil resistance–deflection ($p-y$) behaviour within the Winkler formulation. In order to isolate the effects of soil behaviour on the FFR, as well as the effects of the soil–pile interaction modelling, the gap formation between the soil–pile is not considered. It is worth emphasising that the selected BDWF formulations are not intended to represent the full complexity of soil–pile interaction. Instead, they are deliberately used to isolate how different ways of introducing soil non-linearity (in wave propagation, in the soil–pile springs, or in both) affect the predicted kinematic demand on piles. This allows a consistent and systematic comparison between modelling strategies, rather than the calibration of a single "most realistic" interaction model. In addition, under kinematic loading, the relative displacement between pile and surrounding soil is generally limited, resulting in low contact stresses along the interface. Previous studies (e.g., [27,38]) have shown that, under such conditions, interface effects such as gap formation have a minor influence on the overall response. Therefore, neglecting gap formation allows focusing on the role of soil non-linearity without introducing additional modelling uncertainties. In this way the same radiation damping is assumed for all the investigated BDWF models. In detail, the radiation damping per unit length at the generic depth z_j is computed following Gazetas and Dobry [32] for nearly incompressible soils:

$$c_{rj} = 4D\rho_j V_{sj} \tag{21}$$

where D is the pile diameter, and ρ_j and V_{sj} are the soil density and shear wave velocity at depth z_j at small strains. It is worth noting that radiation damping is assumed to be linear and constant within each layer, disregarding the shear wave velocity variations resulting from changes in the shear modulus in the non-linear soil model. Once the free-field displacements at each desired depth are computed from the linear and non-linear soil models under vertical S-wave propagation (Section 2.1), they are introduced into the system as input motions for the springs and radiation dashpots of each BDWF model (Fig. 4). The different BDWF models characterised by distinct $p-y$ behaviours are described below.

BDWF model based on the Gazetas and Dobry's expression

This model considers the linear expression proposed by Gazetas and Dobry [39] to reproduce the $p-y$ behaviour of the Winkler springs:

$$P = \delta E_{sj}\tilde{y} \tag{22}$$

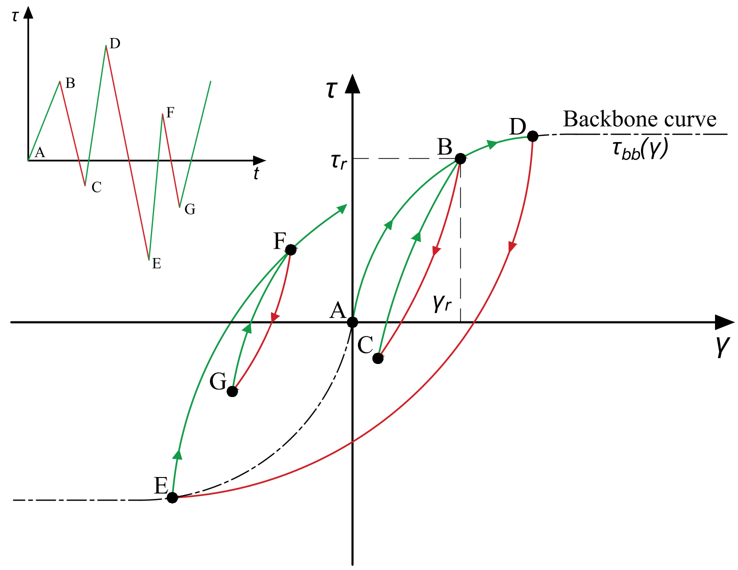

Fig. 3. Cyclic loading example following the extended Masing rules.

being P the soil reaction force per unit length; δ a dimensionless coefficient, typically 1.2 for fixed-head piles embedded in standard soil conditions (see, e.g., [25,39]); E_{sj} the Soil Young's Modulus at depth j; and $\tilde{y}$ the relative soil–pile displacement, which is defined as the difference between the lateral displacement of the pile node (u_n) and that of the soil due to the incident field (u_I), evaluated at each pile node along the pile depth.

BDWF model based on the API recommendation

For this model, the lateral soil resistance–deflection is reproduced by the hyperbolic $p-y$ relationship of sandy soils proposed by the American Petroleum Institute recommendations (API RP 2A-WSD, [18]):

$$P = A\ p_u \tanh\left[\frac{k_{sr} z}{A p_u}\tilde{y}\right] \tag{23}$$

being $A = 0.9$ a dimensionless coefficient for cyclic loading; k_{sr} the initial modulus of subgrade reaction, which can be graphically calculated with the angle of internal friction (Φ_s) following the API recommended practices; and p_u the ultimate bearing capacity at depth z. The ultimate resistance is the minimum of the shallow and deep expressions:

$$p_u = \min(p_{us}, p_{ud}) \tag{24}$$

where:

$$p_{us} = (C_1 z + C_2 D)\Psi_s z \tag{25}$$

and

$$p_{ud} = C_3 D \Psi_s z \tag{26}$$

in which Ψ_s is the effective soil weight; and C_1, C_2, and C_3 are dimensionless coefficients that depend on Φ_s, and can be graphically determined according to the API RP 2A-WSD.

The cyclic behaviour of the hyperbolic $p-y$ relationship is modelled according to the Masing rules previously exposed.

It is important to emphasise that although API curves were developed for offshore applications, they are widely used for deep foundations and are explicitly recognised in bridge design guidelines such as the AASHTO LRFD Specifications [40]. In addition, even though API $p-y$ curves were initially developed from static and low-frequency cyclic lateral load tests, they are one of the most widely used methods for representing depth-dependent soil resistance in pile analysis. Their continued use stems from providing a practical and well-calibrated way to capture non-linear soil–pile interaction in time-domain analyses, while remaining compatible with commonly adopted BDWF models.

BDWF model based on the Gazetas and Dobry's expression considering the variation of the soil Young's modulus

This model extends the Gazetas and Dobry's linear formulation by incorporating the time-dependent degradation of the elastic modulus resulting from the non-linear free-field analysis, assuming that the local (soil–pile interaction) and global (free-field) Young's modulus evolve identically with time. Thus, the $p-y$ relationship becomes:

$$P = \delta E_{sj}(t)\tilde{y} \tag{27}$$

where $E_{sj}(t)$ is the tangent Young's modulus at depth z_j, updated at each time step based on the non-linear stress–strain state of the soil. This model accounts for stiffness degradation but assumes a linear force–displacement relationship at each instant. Therefore, it should be interpreted as an idealised representation of the effect of global stiffness reduction on the local soil–pile response. It is important to note that this expression is not intended as a general constitutive relationship governing local soil response around the pile, but as a modelling tool to assess the sensitivity of the kinematic response to global stiffness degradation effects.

BDWF model based on the API recommendation and scaled with respect to the ultimate shear modulus

To more rigorously couple the non-linear free-field response with the soil–pile interaction behaviour the API $p-y$ curves are scaled according to the following expression:

$$P = A\ p_u \tanh\left[\frac{0.65 G_{uj} k_{sr} z}{G_{0j} A p_u}\tilde{y}\right] \tag{28}$$

where G_{0j} is the initial shear modulus (shear modulus at small-strains), and G_{uj} the ultimate shear modulus of layer j, which is determined as:

$$G_{uj} = \frac{\tau_{uj}}{\gamma_{uj}} \tag{29}$$

where τ_{uj} and γ_{uj} are the peak shear stress and strain reached in the $\tau-\gamma$ hysteresis at layer j, respectively. The 0.65 reduction factor accounts for the fact that peak values are reached ones, while most of the hysteresis behaviour is characterised by lower shear stresses and strains. This factor is conventionally used in soil dynamics practices for defining equivalent linear models, as well as for adjusting backbone curves keeping hysteresis loops within 60 and 70% of the peak stress–strain [41]. This soil–pile interaction model allows relating the API recommended $p-y$ curves with the non-linear soil behaviour under

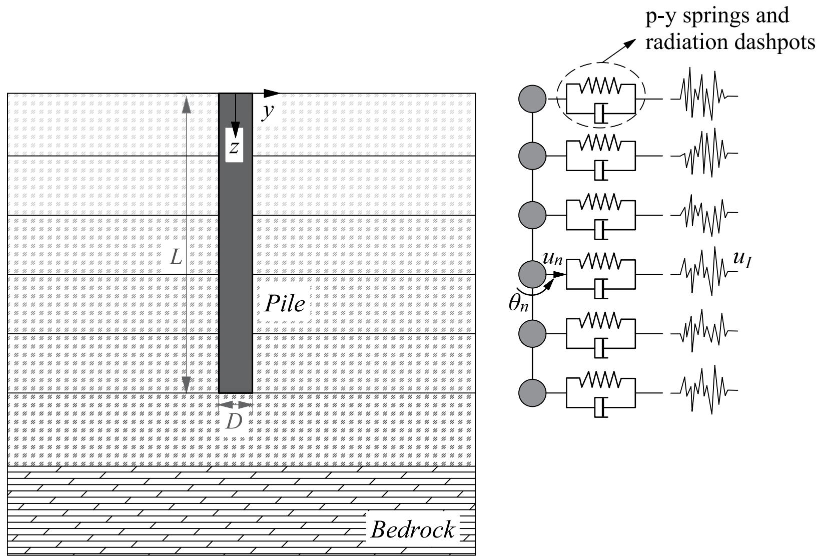

Fig. 4. Pile and soil–structure interaction modelling by BDWF approach.

Table 1
Studied BDWF models and their associated soil behaviours.

BDWF model	$p-y$ relationship	Soil behaviour	Label
Gazetas and Dobry	$P = \delta E_{sj}\, \tilde{y}$	Linear soil model Non-linear soil model	LS-GAZ NLS-GAZ
Gazetas and Dobry considering soil Young's modulus degradation with time	$P = \delta E_{sj}(t)\, \tilde{y}$	Non-linear soil model	NLS-GAZ-DEGR
API RP 2A-WSD	$P = A\, p_u \tanh\left[\frac{k_{sr}\, z}{A\, p_u}\, \tilde{y}\right]$	Linear soil model Non-linear soil model	LS-API NLS-API
Scaled API RP 2A-WSD	$P = A\, p_u \tanh\left[\frac{0.65\, G_{uj}\, k_{sr}\, z}{G_{0j}\, A\, p_u}\, \tilde{y}\right]$	Non-linear soil model	NLS-API-SCAL

vertical S-wave propagation, by incorporating the stiffness degradation through an equivalent shear modulus obtained from the free-field analysis. Thus, it introduces a direct coupling between wave propagation effects and soil–pile interaction behaviour. It is important to note that this expression is introduced as a simplified approach to assess the influence of soil stiffness degradation on the kinematic response.

Table 1 summarises the BDWF models together with the labels used throughout the results section to identify each model. It also indicates the soil constitutive behaviour considered in the analysis of each BDWF model.

2.3. Solutions of the equation of motions

The nodal kinematic variables are computed by solving the global dynamic equation of motion:

$$\mathbf{M}\ddot{\vec{u}}(t) + \mathbf{C}\dot{\vec{u}}(t) + \mathbf{K}\vec{u}(t) = \mathbf{K_{SSI}}(t)\vec{u_I}(t) + \mathbf{C_{SSI}}\dot{\vec{u_I}}(t) \tag{30}$$

being $\vec{u}$, $\dot{\vec{u}}$, $\ddot{\vec{u}}$ the vectors containing the nodal pile displacements, velocities and accelerations; **M**, **C**, **K** the pile mass, and the damping and stiffness matrices of the system composed by the pile and SSI contribution (Winkler springs and dashpots); $\mathbf{K_{SSI}}$ and $\mathbf{C_{SSI}}$ the stiffness and damping matrices of the SSI contribution; and $\vec{u_I}$, $\dot{\vec{u_I}}$ the nodal free-field displacement and velocity vectors due to the seismic excitation. The problem solution is obtained integrating system (Eq. (30)) with the Newmark's method for linear and non-linear systems, assuming the average acceleration within two subsequent time steps. For the non-linear applications, the Newmark's iterative procedure is stopped when the following convergence criterion is fulfilled in terms of displacement differences obtained in each node between two consecutive iterations:

$$|\vec{\Delta u}| \leq 10^{-12} \tag{31}$$

Table 2
Geometrical and mechanical properties of the reinforced concrete piles.

Property	Value
Diameter (D) [m]	2; 5
Length (L) [m]	30
Young's Modulus (E) [GPa]	30
Density (ρ) [kg/m^3]	2500
Damping fraction (ζ_p) [%]	2

3. Problem definition

This section addresses piles, soil profiles and seismic inputs adopted in this work.

3.1. Pile definition

Two reinforced concrete piles with a high and medium slenderness ratio (L/D, obtained by varying the pile diameter D) are examined in this study, representative of common foundation elements used in bridge construction. Their geometrical and mechanical properties are defined in Table 2.

Both floating and end-bearing piles are considered (Fig. 5); the floating pile is assumed to be embedded in a soil overlying an elastic bedrock, whereas the end-bearing one is assumed to have its tip resting on the bedrock, simulating an almost fixed-rotation condition due to the high stiffness contrast. For these end-bearing piles, a rigid bedrock is assumed, ensuring that the pile tip follows the imposed seismic displacement of the bedrock in both soil models. Note that, because

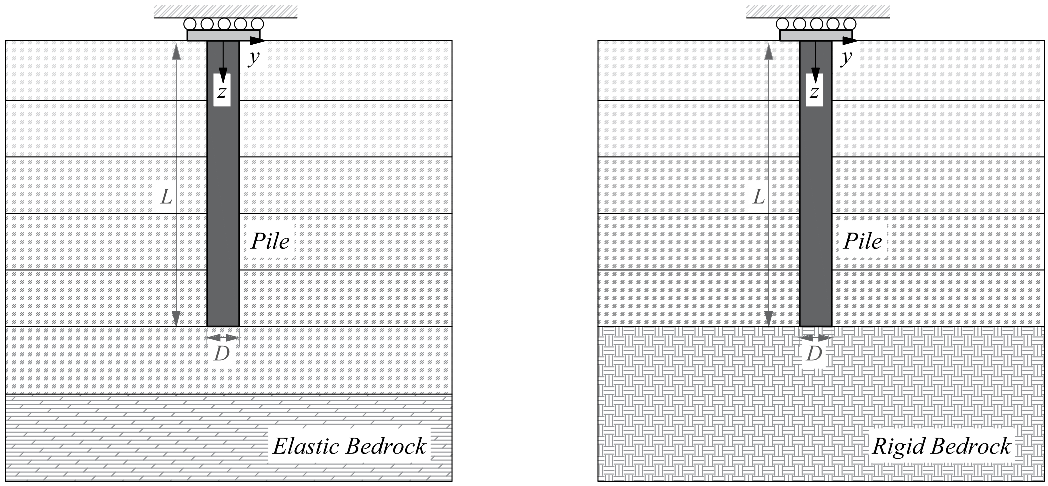

Fig. 5. Floating pile over an elastic bedrock and end-bearing pile over a rigid bedrock.

the excitation is applied at the surface bedrock due to the characteristics of the non-linear soil model (see Fig. 2), the pile-tip boundary conditions become a fundamental aspect that may significantly influence the kinematic response of the pile. All piles are considered to have the rotational degree of freedom restrained at their heads (fixed head). Although this does not fully represent the boundary conditions of single-pile foundations of bridge piers, the adopted schemes and boundary conditions allow investigating the kinematic effects in critical pile cross-sections, such as the interface between soil layers with high impedance contrast and the pile head, where the restraint provided by the structural redundancy as well as by the foundation caps or tie beams usually leads to stress concentrations. Elements with 0.5 m length are used to model all piles, based on a preliminary convergence study.

3.2. Soil definition

Two sandy soil conditions are analysed: a very loose (loose) and a medium dense (dense). Their geotechnical and dynamic properties (including the parameters to capture the non-linear wave propagation model, and the API p–y curves) are presented in Table 3. Representative shear wave velocities of 100 m/s (loose) and 200 m/s (dense) are adopted, consistent with typical values for saturated sands. The bedrock shear wave velocity is taken as 700 m/s to ensure a high stiffness contrast. Parameters for the non-linear soil model are obtained considering a null plasticity index (a typical value adopted for clean sands), through the Vucetic and Dobry relation [42,43] between the secant shear modulus (G/G_0) and shear strain (γ). Finally, parameters for the definition of the BDWF models based on the API recommendation are obtained from the recommended charts based on the soil friction angle.

For each sandy type, two different soil profiles are derived: a homogeneous and non-homogeneous soil profile. The homogeneous one is characterised by a constant reference shear wave velocity along its entire depth. The non-homogeneous soil profiles are described using a power-law variation of shear wave velocity with depth, originally introduced in the form $V_s = cz^n$ by Dobry et al. [44] and later adopted in several studies. The generalised expression used here follows Rovithis et al. [45], who extended the formulation to better reproduce realistic near-surface conditions:

$$V_s(z) = V_{sr}\left(d_s + (1-d_s)\frac{z}{z_r}\right)^n \tag{32}$$

where z is the depth from ground surface; z_r and V_{sr} are the reference depth and shear wave velocity, respectively; $d_s = (V_0/V_{sr})^{1/n}$ is a parameter that defines the shear wave velocity at the ground surface (V_0); and n is the parameter governing the shear wave velocity variation with depth. In this work the values $V_0 = 0$ m/s and $n = 0.5$ are considered, corresponding to a Gibson soil with no stiffness at surface level. The values adopted to define V_0 and n reproduce a soil profile with a linear variation of the Young's modulus, consistent with the API $p-y$ expression (Eq. (23)), where a linear variation of the subgrade reaction modulus is also defined. Although Rovithis et al. [45] provide an exact analytical solution for the free-field response of a linear soil behaviour following the shear wave velocity distribution in Eq. (32), the present study adopts discretised soil models. This approach ensures that the results obtained for the linear soil case can be meaningfully and consistently compared with those from the non-linear one-dimensional lumped soil model.

In order to correlate results from homogeneous and non-homogeneous soil profiles for each soil stiffness and pile layout (floating and end-bearing pile), a reference depth is selected for the non-homogeneous profile that ensures the same fundamental frequency as the homogeneous profile. This choice of establishing the equivalence on the fundamental mode rather than on higher modes (e.g., the second mode) arises from the fact that the first natural frequency is generally the most influential in the seismic response of soft soils (see, e.g., [46]). Tables 4 and 5 present the first three natural frequencies and the reference depth of the soil profiles considered for floating and end-bearing piles, respectively. These natural frequencies were obtained by solving the eigenvalue problem after assembling the soil stiffness and mass matrices derived from the one-dimensional lumped model shown in Fig. 2, assuming the initial stiffness of each soil layer.

Each soil profile is discretised into uniform soil layers of 0.5 m depth for computing the FFR under vertical S-wave propagation in the same position of the pile mesh. This discretisation level was selected based on a preliminary convergence analysis, in which the FFR obtained with the linear discretised soil model was compared against the analytical FFR solution proposed by Rovithis et al. [45], showing very good agreement. Fig. 6 shows the variation of the shear wave velocity with depth for each soil profile, where blue and red lines are used for the homogeneous and non-homogeneous soil profiles, respectively. In the first and second rows the soil profiles for the floating and end-bearing pile cases are shown accordingly. As shown in Fig. 6, the soil profile extends down to 40 m for the floating pile and to 30 m for the end-bearing pile.

Fig. 7 depicts the first three normalised modal shapes of the homogeneous (blue lines) and non-homogeneous (red lines) profiles. Profiles relevant to the floating and end-bearing piles configurations are shown with continuous and dashed lines, respectively. As expected, modal shapes of the homogeneous soil profiles have a zero-shear strain at ground surface (the modal shape at the free surface presents a vertical tangent). On the contrary, for non-homogeneous soil profiles shear strain at ground surface tends to infinite (horizontal tangent): this is

Table 3
Geotechnical properties and model parameters for the sandy soils studied in this work.

Parameter	Very loose sand (Loose)		Medium dense sand (Dense)
Poisson's ratio (ν_s)		0.49	
Density (ρ_s) [kg/m^3]		2000	
Reference shear wave velocity (V_{sr}) [m/s]	100		200
Damping fraction (ζ_s) [%]		2.5	
Bedrock Properties			
Shear wave velocity (V_{sB}) [m/s]		700	
Density (ρ_B) [kg/m^3]		2000	
Modified Kondner–Zelasko Model Parameters			
β		1	
s		0.81	
Reference effective shear strain (γ_{Ref}) [%]		0.03	
Reference effective vertical stress (σ'_{Ref}) [kPa]		100	
b		0.3	
Parameters for the SSI proposed by the API recommendation			
Angle of internal friction (Φ_s) [°]	28		36
Initial modulus of subgrade reaction (k_{sr}) [MN/m^3]	4.07		25.79
C_1	1.6		3.3
C_2	2.4		3.6
C_3	22		60

Table 4
First three natural frequencies and reference depth of the soil profiles considered for the floating piles.

	Loose soil		Dense soil	
Mode	Homogeneous	Non-homogeneous	Homogeneous	Non-homogeneous
1st (Hz)	0.625	0.625	1.250	1.249
2nd (Hz)	1.875	1.428	3.749	2.857
3rd (Hz)	3.124	2.210	6.247	4.420
Reference depth (z_r) [m]		23.45		

Table 5
First three natural frequencies and reference depth of the soil profiles considered for the end-bearing piles.

	Loose soil		Dense soil	
Mode	Homogeneous	Non-homogeneous	Homogeneous	Non-homogeneous
1st (Hz)	0.833	0.833	1.667	1.666
2nd (Hz)	2.499	1.899	4.999	3.799
3rd (Hz)	4.164	2.904	8.327	5.808
Reference depth (z_r) [m]		17.57		

consistent with the soil stiffness in the shallower layers that is very low in this case. These trends are in agreement with other works, such as, [45,47].

3.3. Seismic signals

Ten different seismic signals are used in this work to compute the pile kinematic response. Table 6 presents the main information about each seismic signal: the database record sequence number (RSN), the orientation of the horizontal component relative to the north, earthquake event name and year, station name where they were measured, the average shear wave velocity in the upper 30 m depth ($V_{s,30}$) of the soils in which they were recorded, and the Peak Ground Acceleration (PGA) of each signal. All seismic signals are scaled to obtain three different PGAs (0.2, 0.4 and 0.6 g) in order to investigate different scenarios ranging from medium to strong intensity earthquakes. The seismic response of the piles are quantified in terms of mean envelopes obtained from the ten seismic signals. The selected input motions, characterised by different frequency contents (see Fig. 8), allow investigation of the soil–pile system response while accounting for the system's sensitivity to the varying frequency content of the input.

With the aim of removing spurious trends in each seismic signal, a second order polynomial baseline correction has been applied to all earthquake records. In addition, to obtain accurate non-linear responses, a time step of $2.5 \cdot 10^{-3}$ s has been selected for computing all responses after a convergence evaluation; this makes it possible to accurately capture the velocity reversal point in the hysteretic cycles of the non-linear models.

4. Results and discussion

In order to discuss and analyse the distinct effects of soil response under seismic S-wave propagation, as well as the effect of different modelling strategies for the soil–pile system (BDWF models) on the kinematic response of both floating and end-bearing piles in different soil profiles, results are organised as follows: firstly, the FFR of the different soil profiles under vertical S-wave propagation is shown and discussed; secondly, the kinematic pile response, expressed in terms of bending moment and shear force envelopes obtained for all pile–soil systems are evaluated.

4.1. Free-field soil response

Fig. 9 shows the FFRs of the different soil profiles under vertical S-wave propagation considering both linear and non-linear soil behaviours. The FFRs are presented in terms of envelopes of maximum soil accelerations (first pair of columns), shear strains (second pair of

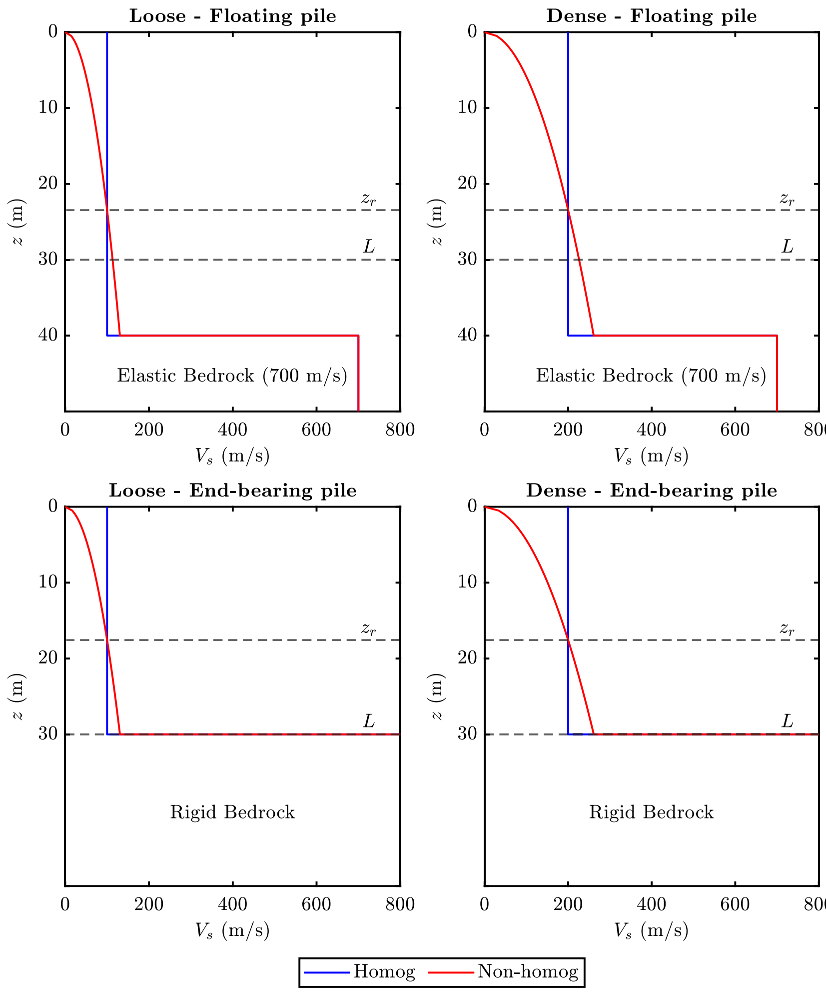

Fig. 6. Variation of the shear wave velocity with depth for each soil profile.

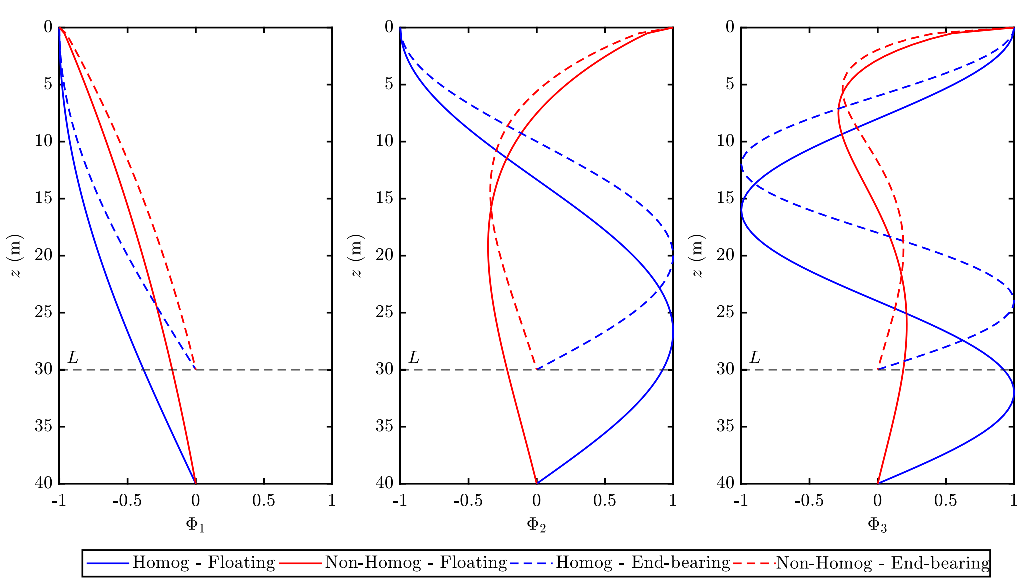

Fig. 7. First three normalised modal shapes of each soil profile.

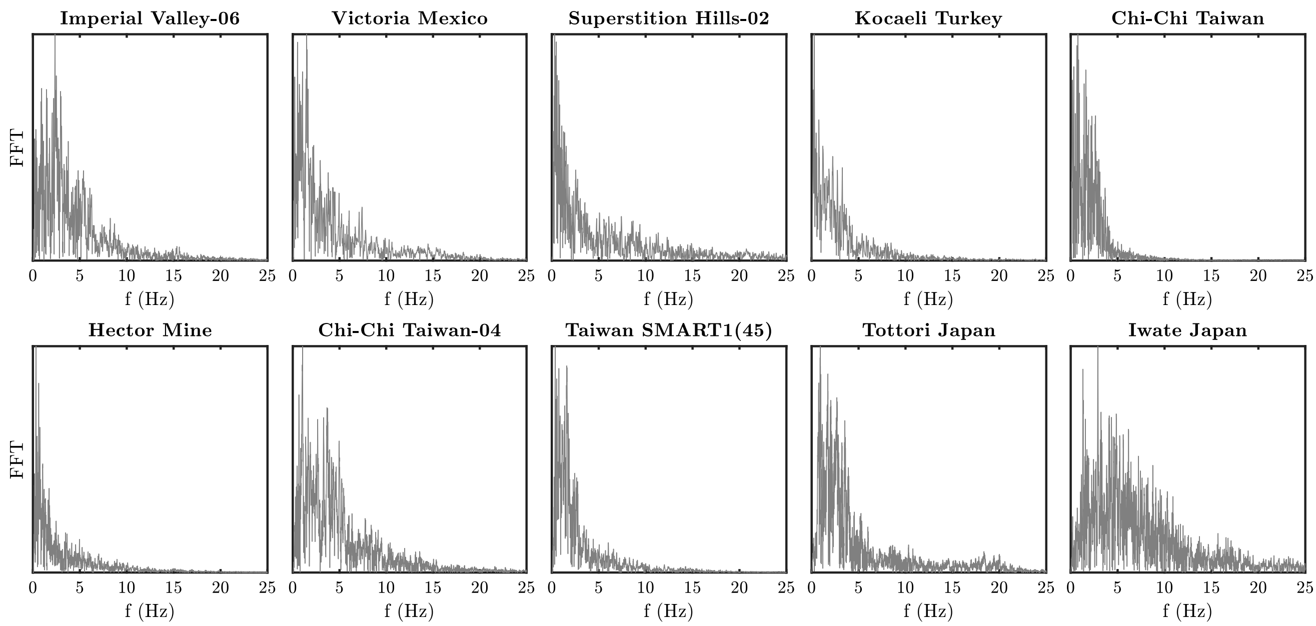

Fig. 8. Normalised frequency content (FFT) of the accelerograms adopted in this study.

Table 6
Seismic signals (accelerograms) used in this work.
Source: [48].

RSN	Dir. (°)	Event name	Year	Station name	$V_{S,30}$ (m/s)	PGA (g)
186	90	Imperial Valley-06	1979	Niland Fire Station	212	0.11
266	102	Victoria Mexico	1980	Chihuahua	242	0.15
729	0	Superstition Hills-02	1987	Imperial Valley W.L.A	179	0.21
1176	60	Kocaeli Turkey	1999	Yarimca	297	0.23
1498	59	Chi-Chi Taiwan	1999	TCU059	273	0.16
1792	90	Hector Mine	1999	Indio-Riverside C.F.G	282	0.12
2715	47	Chi-Chi Taiwan-04	1999	CHY047	170	0.13
3683	11	Taiwan SMART1(45)	1986	SMART1 O11	295	0.13
3965	8	Tottori Japan	2000	TTR008	139	0.32
5666	7	Iwate Japan	2008	MYG007	167	0.13

columns), and envelopes of minimum shear modulus ratio (G/G_0) for the non-linear model only (third pair of columns). For all these response variables, the mean values obtained from the ten seismic signals are presented. The envelopes computed in the homogeneous and non-homogeneous soil profiles are shown in the first and second columns of each pair of columns accordingly. Furthermore, each subgraph is divided into two parts by a black dash-dot line, and the envelopes obtained for the dense and loose soils are reported in the left and right sides of the dash-dot line, respectively. Finally, results corresponding to the set of earthquakes scaled to obtain PGAs of 0.2, 0.4 and 0.6 g are disposed on rows; in order to compare results from earthquakes with different intensity, free-field accelerations and shear strains are normalised with respect to the relevant PGA, enabling comparison across the three shaking intensities. Results obtained for the linear and non-linear soil models under S-wave propagation (denoted with labels LS and NLS in the figure legend) are depicted with blue and red lines, respectively. In addition, the FFRs of soil profiles relevant to the floating and end-bearing piles are shown using continuous and dashed lines, respectively.

Results of Fig. 9 show notable differences between the FFRs computed from the different soil models. Comparing the free-field shear strain and acceleration envelopes obtained for the linear and non-linear soil models (blue and red lines, accordingly), it can be noted that the envelopes obtained for the linear soil assumption are quite greater than those of the non-linear soil model. This behaviour can be explained by the mechanisms associated with non-linear soil response. First, hysteretic stress–strain relationships introduce additional energy dissipation through hysteretic damping, which attenuates the propagating seismic waves, reducing their amplitude and the resulting shear strains. Second, the degradation of shear modulus with increasing strain reduces the shear wave velocity, altering the impedance profile of the soil column. Consequently, the shift of the soil's natural frequencies to lower values drives the response towards frequency ranges characterised by lower energy content. The combined effect of these mechanisms produces a more attenuated wave field and, consequently, smaller free-field shear strain and acceleration envelopes in the non-linear soil model. However, it is important to note that the kinematic response of piles is not governed only by the amplitude of shear strain, but rather by their gradient within the soil profile, which is responsible for the pile curvature. In non-linear soil conditions, even if strain amplitudes are reduced, stiffness degradation may lead to sharper variations of the shear strain profile, resulting in increased curvature demands and kinematic bending moments in piles.

Under the linear assumption (blue lines), acceleration envelopes for both profile types (homogeneous and non-homogeneous) increase as deep decreases. In the non-homogeneous profile, the amplification seems to be more pronounced due to the stronger stiffness gradient (stiffness decreases as deep decreases). Nevertheless, the non-linear model (red line) presents an opposite trend: surface accelerations decrease with depth reduction, consistent with stiffness degradation and hysteretic damping developing primarily in deeper layers and attenuating the propagation of motion upward.

This can be observed in the free-field shear strain envelopes of the homogeneous soil profile in which the maximum shear strains are

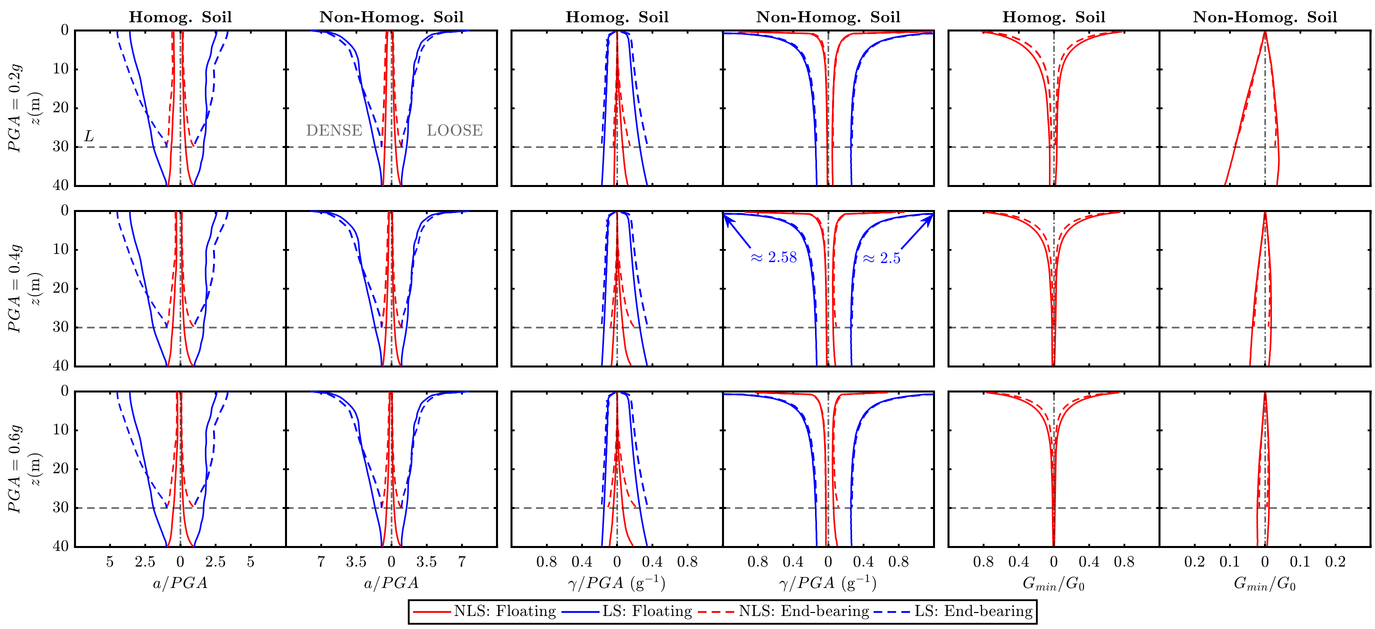

Fig. 9. Free-field response for all considered soil behaviours and profiles.

obtained in the deepest soil layer, progressively reducing towards the surface. However, in the non-homogeneous soil profile, the maximum shear strains are reached near the ground surface due to the progressive reduction of shear wave velocities and stiffness in the shallower layers. This behaviour can be interpreted based on the associated modal shapes presented in Fig. 7, which show that in inhomogeneous profiles the deformation tends to concentrate near the surface, where the soil is more compliant. In contrast, homogeneous soil profiles exhibit a more uniform distribution of stiffness with depth, leading to smoother modal shapes and deeper locations of maximum shear strain. These observed mechanisms are also consistent with those reported by Rovithis et al. [45], who show that soil non-homogeneity not only modifies the effective stiffness but also alters the modal shape geometry, leading to a higher concentration of strains and dynamic amplitudes near the surface. In the case of the non-homogeneous soil profile and non-linear soil model, the variation in shear strain from a depth of 10 m to the final depth is noticeably less pronounced compared to the homogeneous profile. Note that in the non-homogeneous soil profiles the deeper layers present a great stiffness, leading to a lesser degradation than in the homogeneous profile.

The envelopes of the minimum shear modulus ratio present trends in line with above considerations: homogeneous soil profiles imply a greater degradation (lower shear modulus ratios) at deeper layers, whereas in non-homogeneous profiles higher degradation is reached at shallower layers. Furthermore, in accordance with prior expectations, higher degradation is obtained for higher PGAs.

It is worth mentioning that, in agreement with theoretical predictions, the same scaled accelerations and shear strain envelopes are obtained for the different PGAs in case of linear soil models. In addition, for the scaled envelopes corresponding to the non-linear soil model similar envelopes are generally obtained, with apparently few minor differences due to the excitation magnitude.

4.2. Pile kinematic responses

4.2.1. Floating pile

Figs. 10 and 11 present the mean envelopes of absolute bending moments and shear forces of the floating piles for all considered soil behaviours, soil profiles, and BDWF models. The envelopes obtained for the two pile diameters are shown by pair of columns. For each pile diameter, results from the homogeneous and non-homogeneous soil profiles are disposed in the first and second columns, respectively. As in Fig. 9, results for each PGA are shown by rows, and the envelopes corresponding to the dense and loose soils are presented in the left and right sides of each subgraph, respectively, separated by a vertical dash-dot line. The envelopes obtained for the non-linear and linear soil response under S-wave seismic propagation are presented with continuous and dashed lines, respectively. Additionally, the different investigated BDWF models are shown with different colours.

From the analysis of Figs. 10 and 11, some general trends of bending moments and shear forces envelopes for the floating pile can be observed. For instance, remarkable different envelopes are obtained between the non-linear and linear soil models (LS vs NLS; continuous vs dashed lines). This becomes evident when comparing the envelopes of the same BDWF model for both linear and non-linear soil behaviours (NLS-API vs LS-API; and NLS-GAZ vs LS-GAZ). Thus, the pile kinematic response is highly influenced by the soil modelling adopted for the evaluation of the FFR. Generally, the soil non-linearity leads to greater envelopes than those resulting from the linear assumption, except for the bending moment envelopes computed for the homogeneous soil profile at shallower depths (approximately first ten metres of depth), where the linear soil behaviour leads to higher bending moments. This difference is mainly related to the depth distribution of non-linearity within the soil profile and its effect on the free-field displacement profile. Note that although the free-field shear strains for the non-linear soil model are lower than those obtained for the linear model (Fig. 9), their gradient with depth is higher. This leads to larger pile curvatures, which are responsible for higher kinematic bending moments and shear forces. This occurs because, in homogeneous soils, most of the non-linear behaviour concentrates at greater depths (where the highest shear stains are attained), whereas in non-homogeneous soils it develops in shallower layers (as a consequence of the lower soil properties). The concentration of non-linearities in these zones is responsible for high shear strain gradients with depth. From the SSI perspective, the response is controlled by two competing effects: (i) the free-field displacement profile, which drives the kinematic demand, and (ii) the stiffness of the soil–pile interacting mechanism, which controls the soil–pile interaction forces. By focusing on the BDWF models on non-linear soils, the consideration of the soil Young's modulus degradation within the SSI modelling (NLS-GAZ-DEGR) provides smaller responses than those obtained by disregarding this issue (NLS-GAZ). This behaviour

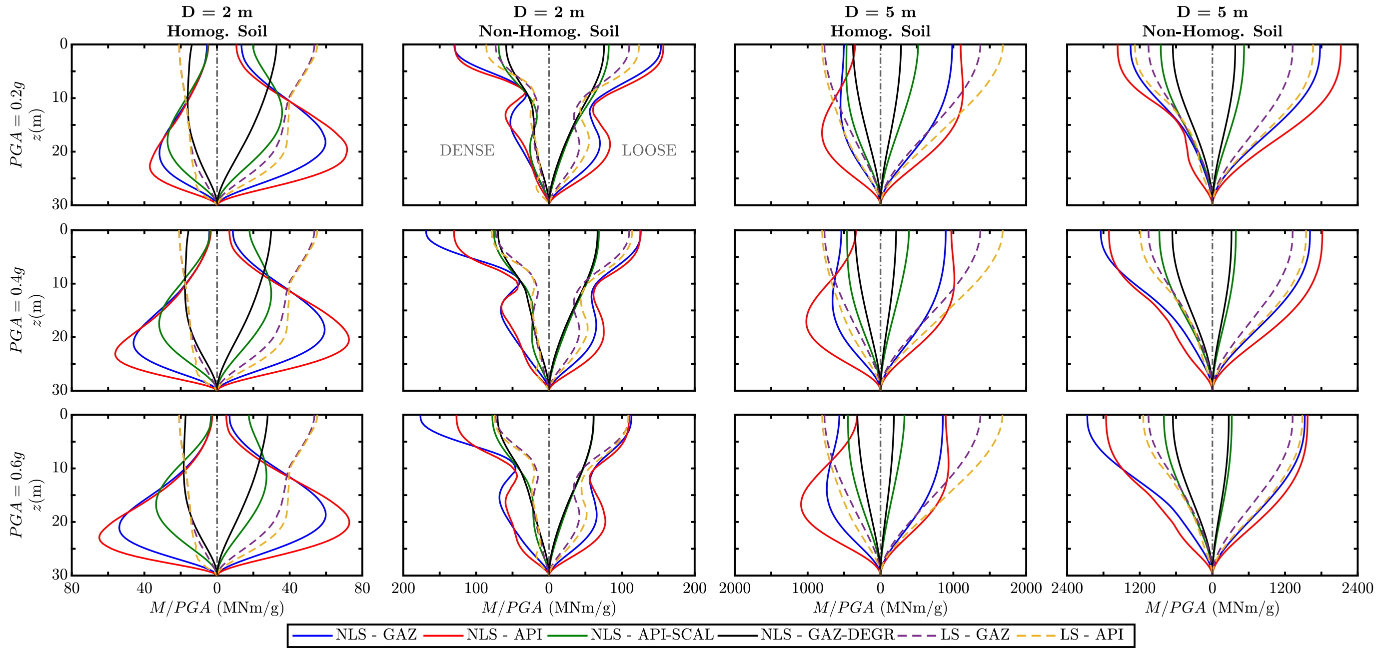

Fig. 10. Bending moments envelopes for all considered soils and BDWF models (floating pile).

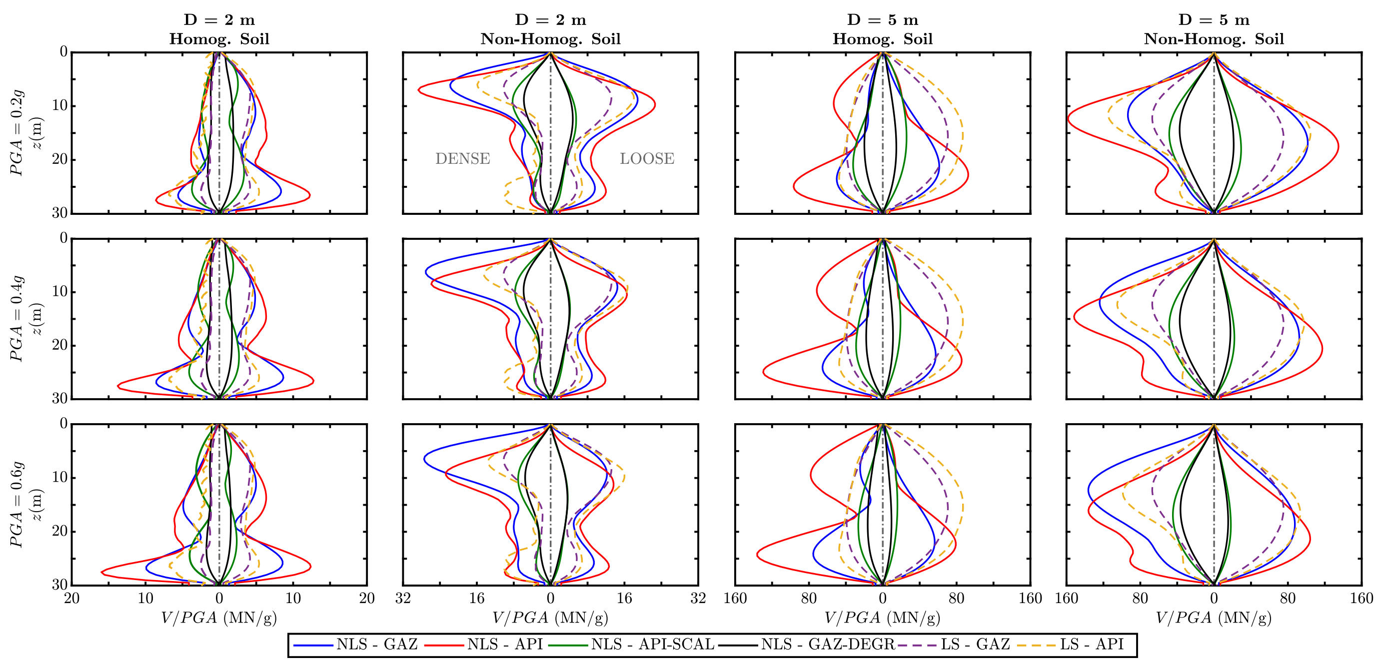

Fig. 11. Shear forces envelopes for all considered soils and BDWF models (floating pile).

can be physically interpreted by considering that stiffness degradation in the soil reduces the soil–pile interaction forces, resulting in lower internal forces. Only in specific cases (e.g., small diameter piles in homogeneous dense soils at shallow depths), the NLS-GAZ-DEGR model may lead to slightly higher responses, due to localised variations in the displacement field. In addition, scaling the API $p-y$ curves (NLS-API-SCAL) generally leads to results like those achieved with the NLS-GAZ-DEGR model. This is consistent with the fact that reduced soil stiffness limits the soil–pile interaction forces, even when the free-field motion is significant. Among the four BDWF models studied for the non-linear soil behaviour, those producing the higher envelopes are the models based on the API $p-y$ curves and Gazetas and Dobry's expression (NLS-API and NLS-GAZ). Furthermore, if the API and GAZ BDWF models are compared in both soil behaviours (NLS-API vs NLS-GAZ, and LS-API vs LS-GAZ), it is noted that the API BDWF assumption generally leads to higher envelopes than the GAZ one in both soil behaviours. This effect is related to the different representation of soil non-linearity in the two approaches. Although the non-linear formulation based on the API approach introduces hysteretic damping into the system, the degradation of SSI stiffness under cyclic loading can still lead to increased lateral displacement gradients along the pile, particularly in zones where non-linearities are more pronounced. As a result, even with energy dissipation, the API-based formulation may produce higher local curvature demands and, consequently, larger internal forces in the pile. Regarding the influence of the different PGAs, similar scaled envelopes are generally obtained in the loose soils

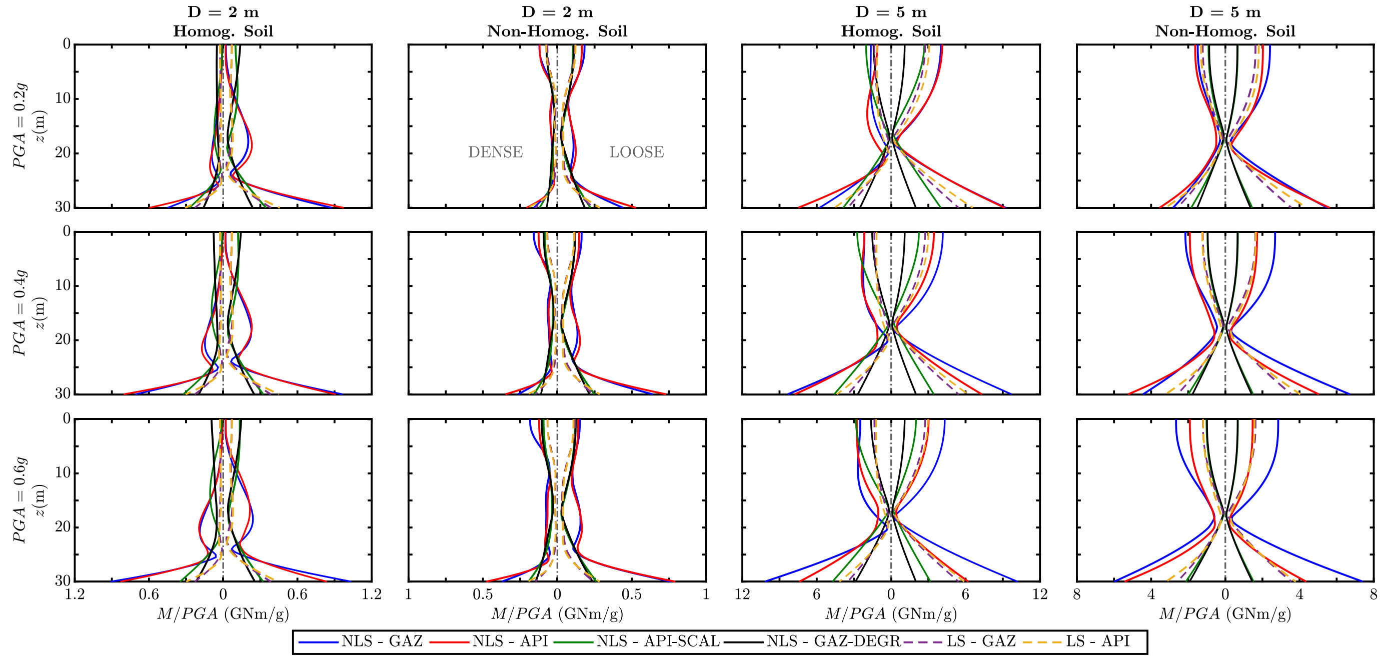

Fig. 12. Bending moments envelopes for all considered soils and BDWF models (end-bearing pile).

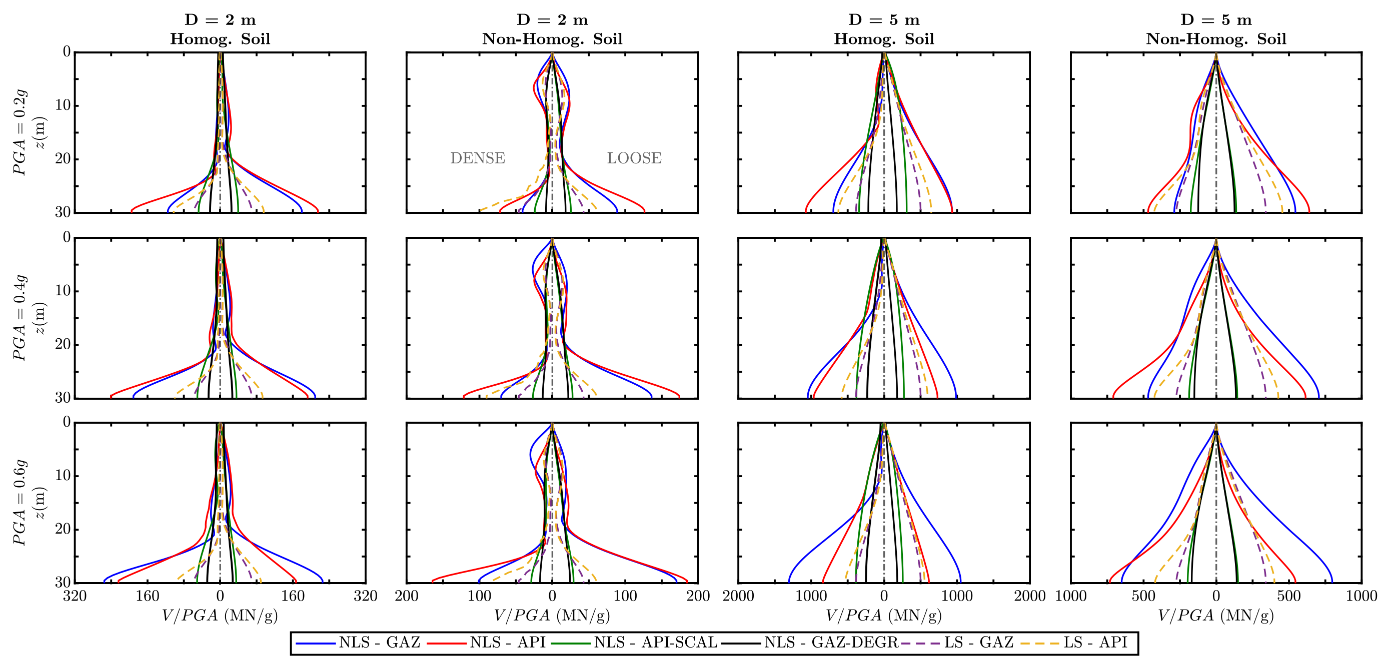

Fig. 13. Shear forces envelopes for all considered soils and BDWF models (end-bearing pile).

for all cases. Nevertheless, in the dense soil, the scaled envelopes of the NLS-GAZ and NLS-API cases, tend to significantly vary, increasing their envelopes as the maximum seismic acceleration increases. The other envelopes of non-linear soil behaviour (NLS-GAZ-DEGR and NLS-API-SCAL) remain practically consistent as the PGA increases. Again, as expected, the same scaled envelopes are obtained for the LS-GAZ model by varying the PGAs, in view of the problem linearity. In addition, the envelopes of the remaining linear model (LS-API) are practically similar for all the PGAs.

From an overall point of view, envelopes of bending moments in Fig. 10 reveal that the maximum values are reached at surface level if a linear soil model is considered. Differently, for non-linear soil behaviour, peak bending moments are obtained at surface when the soil is non-homogeneous, and at deeper layers when the soil is homogeneous. This is consistent with results shown in Fig. 9 in terms of shear strains; indeed, higher shear strains (triggering high non-linearities) appear at surface level of the non-homogeneous soils, whereas for homogeneous soils greater shear strains are given at deeper depths. Besides, for homogeneous soil profiles with a non-linear behaviour, the maximum bending moment values are reached in shallower layers as the stiffness (diameter) of pile increases. From the comparison of the different BDWF models, it comes out that similar results between the linear and non-linear BDWF models (LS-GAZ and LS-API) are generally obtained when a linear behaviour of soil is considered. Conversely, for the non-linear soil behaviour, more differences between these two BDWF models (NLS-GAZ and NLS-API) are identified, especially in homogeneous soils and by increasing the PGA. Finally, comparing the bending moment envelopes of the loose and dense soils, it is observed that the loose soil conducts to higher envelopes when a linear soil behaviour is considered. However, for the non-linear soil behaviour, a clear trend regarding this aspect is not found.

As for the envelopes of scaled shear forces (Fig. 11), it is observed that in homogeneous soil profiles the maximum shear forces are reached at deeper layers, for both soil behaviours (linear and non-linear). Conversely, in non-homogeneous soil profiles the maximums are given at shallower layers. These trends are consistent with the discussion of the FFR presented earlier (Fig. 9). In addition, the shear force envelopes reveal more pronounced differences between the GAZ and API BDWF models for both soil behaviours, compared with the corresponding bending moment envelopes.

4.2.2. End-bearing pile

Figs. 12 and 13 present the envelopes of the mean absolute bending moments and shear forces for the end-bearing pile, for all the soil behaviours, soil profiles, and BDWF models. Both Figures are presented following the same arrangement of Figs. 10 and 11 relevant to the floating pile. Regarding the shape of the envelopes, consistent with expectations, the maximum bending moment and shear force values are reached at the interface with the bedrock, where the maximum impedance contrast between the layers is found. Concerning the general trends obtained for both envelopes, similarly to floating pile envelopes, high differences are identified comparing the behaviour of similar BDWF models in non-linear and linear soil layers (NLS-API vs LS-API; and NLS-GAZ vs LS-GAZ). Thus, the approach adopted for modelling the propagation of vertical S-wave plays a crucial role in the pile kinematic response. Generally, it is observed that the non-linear soil assumption leads to conservative envelopes. Nevertheless, when the BDWF models that account for shear modulus degradation and scaled API $p-y$ curves (NLS-GAZ-DEGR and NLS-API-SCAL) are compared with those assuming linear soil behaviour (LS-GAZ and LS-API), the latter generally produce similar or even greater values of the maximum internal forces. Among the BDWF models including a non-linear soil behaviour, the NLS-GAZ and NLS-API models are those producing the highest envelopes. The remaining two BDWF models addressing the soil non-linearities (NLS-GAZ-DEGR and NLS-API-SCAL) lead to similar results in the non-homogeneous soil profiles, generally being the NLS-API-SCAL model more conservative. Furthermore, for the linear soil-behaviour envelopes, the LS-API model yields larger envelopes than the LS-GAZ model. These overall trends in the internal force envelopes of the end-bearing pile were similarly observed for the floating pile. As for the influence of PGA, it can be observed that for a non-linear soil behaviour, the envelopes obtained with the NLS-GAZ model show a positive correlation with increasing peak seismic acceleration. In contrast, this trend is not totally observed in the NLS-API model. For instance, in some cases, such as the largest pile diameter embedded in the homogeneous soil profile or in the loose non-homogeneous profile, the scaled envelopes obtained in the NLS-API model decrease as the PGA increases. This occurs because a more pronounced non-linear behaviour develops as the excitation level increases, enhancing hysteretic damping and thereby reducing the excitation transmitted to the pile.

Regarding the scaled mean bending moments (Fig. 12), it is observed that similar envelopes between the API and GAZ BDWF models are obtained for both soil behaviours. Significant differences between these two BDWF models are only noticeable for the non-linear soil behaviour and the highest pile diameter and peak seismic accelerations. For this case (non-linear soil behaviour, and largest pile diameter and seismic acceleration), the GAZ BDWF model generally leads to greater envelopes than those obtained in the API one. Thus, for an end-bearing pile, a linear BDWF model based on the expression proposed by Gazetas and Dobry provides a reliable and computationally efficient approach for estimating kinematic bending moments. Finally, concerning the scaled mean shear forces (Fig. 13), more differences can be noticed between the API and GAZ BDWF models for both soil behaviours under vertical S-wave propagation (linear and non-linear).

5. Conclusions

This study examined the kinematic seismic response of single-pile bridge foundations by systematically investigating the combined effects of soil behaviour under vertically propagating S-waves and different modelling strategies for soil–pile interaction within the BDWF framework. Linear and non-linear soil models were used to evaluate free-field response, while several BDWF formulations were adopted to represent soil–pile interaction. Floating and end-bearing piles embedded in homogeneous and non-homogeneous sandy deposits were analysed under a set of ten earthquake records scaled to different intensity levels.

The results show that soil non-linearity in wave propagation plays a primary role in controlling pile kinematic demand. Non-linear free-field response significantly modifies both the amplitude and depth distribution of soil deformations and, in many cases, governs bending moments and shear forces more strongly than the specific formulation adopted for the soil–pile springs. Consequently, assuming linear site response may lead to non-conservative estimates of kinematic demand.

Among the investigated BDWF formulations, models based on API p-y curves and on the Gazetas and Dobry expression generally produced the largest envelopes when combined with non-linear free-field response. Introducing soil stiffness degradation into the springs reduced internal forces, indicating that neglecting degradation at the soil–pile interface is usually conservative, whereas neglecting non-linear site response is not.

A further key outcome is that the depth of maximum bending moments is primarily controlled by where soil non-linearity concentrates within the deposit. In homogeneous profiles, peak demand tends to develop at depth, while in strongly non-homogeneous profiles it shifts towards shallower layers.

The findings highlight the importance of explicitly accounting for non-linear site response in the seismic kinematic assessment of deep foundations. The study is limited to vertically propagating S-waves and kinematic interaction only; future work should address the combined effects of inertial interaction, multidirectional input and more advanced soil–pile constitutive models.

CRediT authorship contribution statement

Eduardo Rodríguez-Galván: Writing – original draft, Visualization, Software, Methodology, Conceptualization. **Sandro Carbonari:** Writing – review & editing, Supervision, Conceptualization. **Francesca Dezi:** Writing – review & editing, Supervision, Conceptualization. **Guillermo M. Álamo:** Writing – review & editing, Supervision, Conceptualization. **Juan J. Aznárez:** Writing – review & editing, Supervision, Funding acquisition, Conceptualization. **Orlando Maeso:** Writing – review & editing, Supervision. **Graziano Leoni:** Writing – review & editing, Supervision.

Declaration of competing interest

The authors declare that they have no known competing financial interests or personal relationships that could have appeared to influence the work reported in this paper.

Acknowledgments

This research has been funded by the Ministerio de Ciencia Innovación y Universidades and the Agencia Estatal de Investigación (MICIU/AEI/10.13039/501100011033) of Spain and ERDF/EU through grant PID2023-151635OB-I00 and predoctoral research scholarship PRE2021-099200 (E. Rodríguez-Galván), also funded by FSE+. The research scholarship also provided financial support for a short-term research stay at Università Politecnica delle Marche carried out by E. Rodríguez-Galván.

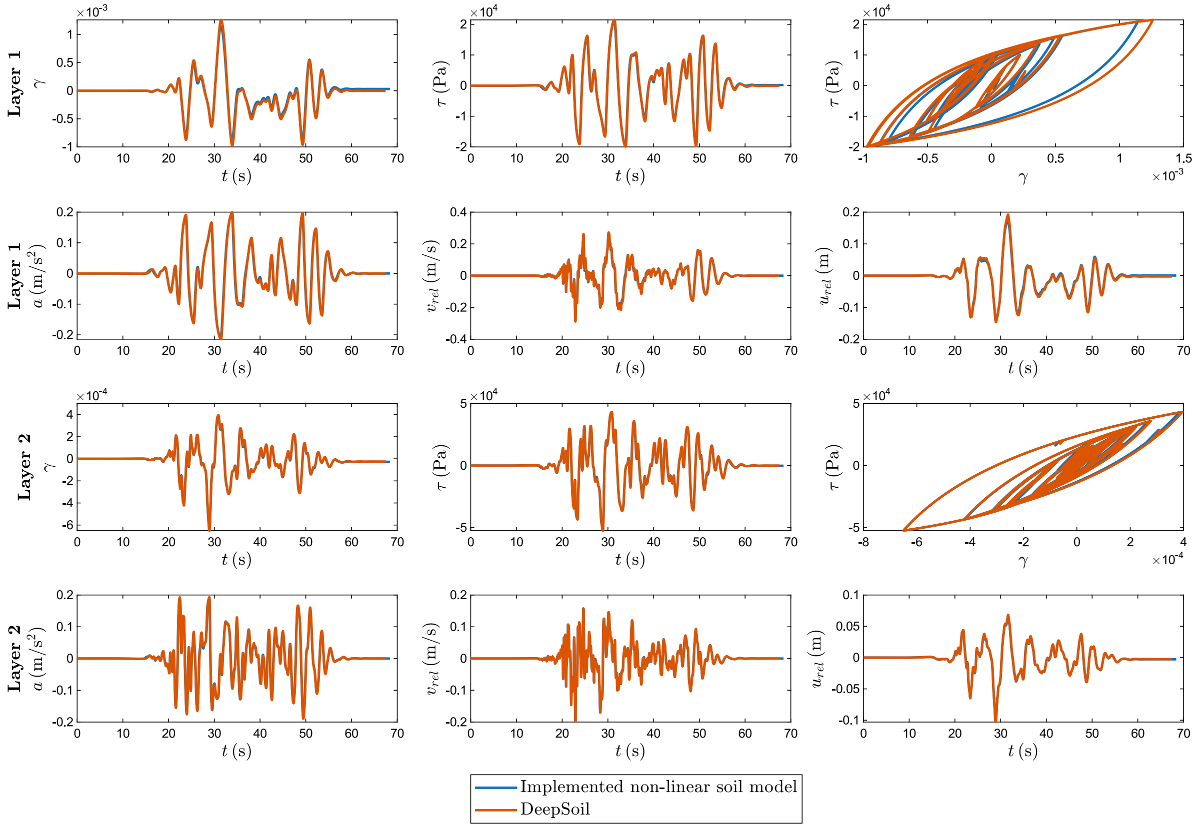

Fig. A.14. Validation of the implemented non-linear one-dimensional soil model vs DeepSoil. Elastic bedrock consideration.

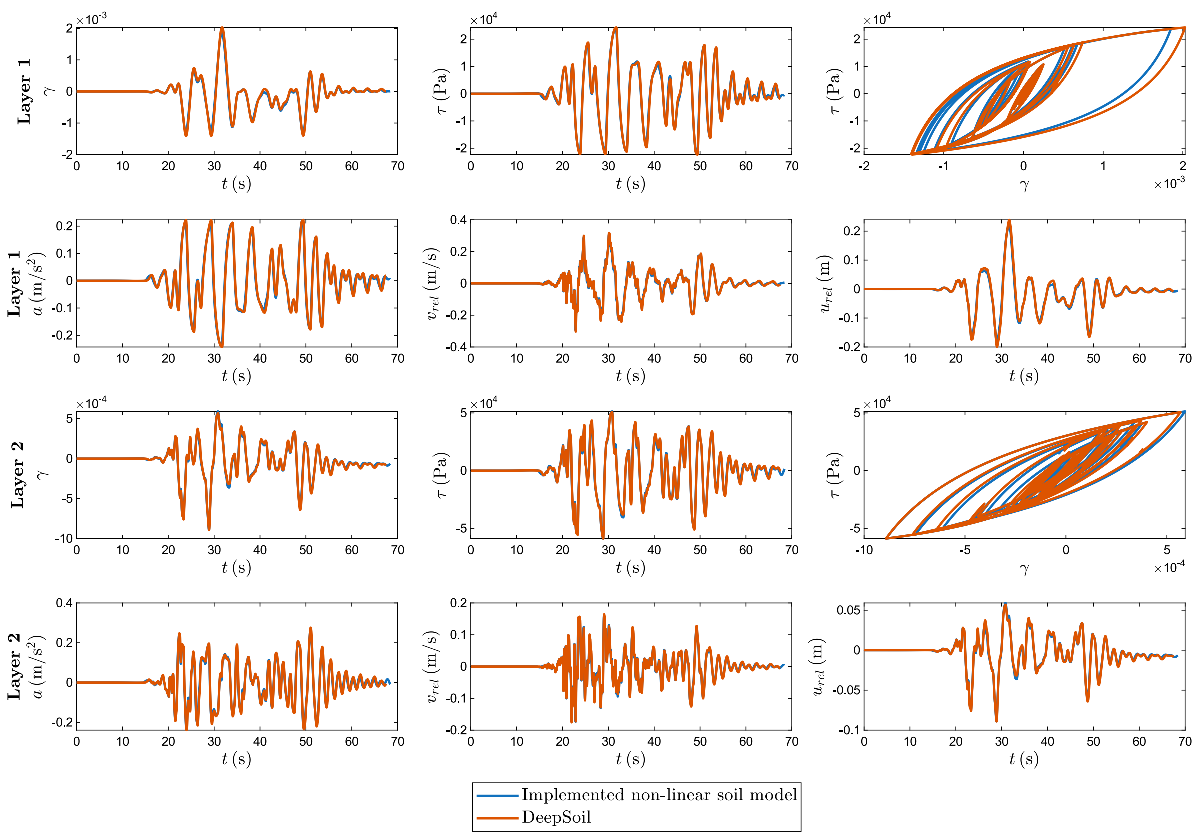

Fig. A.15. Validation of the implemented non-linear one-dimensional soil model vs DeepSoil. Rigid bedrock consideration.

Table A.7
Soil parameters used to validate the non-linear one-dimensional soil model.

Parameter	Layer 1	Layer 2
Shear wave velocity (V_s) [m/s]	200	350
Damping fraction (ζ) [%]	1	
Density (ρ_s) [kg/m^3]	2000	
Layer thickness (h) [m]	100	
Bedrock Properties		
Shear wave velocity (V_{sB}) [m/s]	500	
Density (ρ_B) [kg/m^3]	2000	
Modified Kondner–Zelasko Model Parameters		
β	1.5	
q	0.9	
Reference effective shear strain (γ_{Ref}) [%]	0.0462	
Reference effective vertical stress (σ'_{Ref}) [kPa]	180	
b	0	

Appendix. Non-linear one-dimensional soil model validation

The implemented non-linear one-dimensional soil model under vertical S-wave propagation has been validated with the numerical code DeepSoil v7.1 [37]. For performing this validation two simple examples has been carried out, considering the Imperial Valley-06 seismic excitation (see Table 6) scaled with respect to a maximum ground acceleration of 0.2 g. The first validation case considers a simple soil composed of two layers with different shear wave velocities and an elastic bedrock. The other one maintains all the same properties but considering a rigid bedrock. Table A.7 describes the soil parameters used to perform the validation of the implemented non-linear and one-dimensional model.

Figs. A.14 and A.15 shows the results of the validation for the cases of a elastic bedrock and a rigid one respectively. Both Figures presents the FFR of the two layers by pair of rows. The first row of each pair presents the shear strain and stress evolution with time, and the shear stress–strain hysteresis loops. The second row of each layer presents the absolute accelerations evolution with time, and the relative velocities and displacements evolutions with respect to the bedrock. With a blue colour the results of the implemented non-linear model are shown, whereas with a orange one those corresponding to the DeepSoil. As shown in both figures, the implemented model produces responses that closely match those obtained with DeepSoil. Some differences are observed only in the evolution of the shear stress–strain hysteresis loops. These differences are likely attributable to slight variations in the non-linear iterative solution strategies employed by the two models.

Data availability

Data will be made available on request.

References

[1] Das BM. Principles of foundation engineering. 8th ed. Boston, MA: Cengage Learning; 2015, .
[2] Tomlinson MJ, Woodward J. Pile design and construction practice. 6th ed. Taylor & Francis Group: CRC Press; 2015, .
[3] Mylonakis G, Gazetas G. Seismic soil-structure interaction: beneficial or detrimental? J Earthq Eng 2000;4(3):277–301.
[4] McKenna F. OpenSees: a framework for earthquake engineering simulation. Comput Sci Eng 2011;13(4):58–66.
[5] Álamo GM, Martínez-Castro AE, Padrón LA, Aznárez JJ, Gallego R, Maeso O. Efficient numerical model for the computation of impedance functions of inclined pile groups in layered soils. Eng Struct 2016;126:379–90.
[6] Kaynia AM, Kausel E. Dynamics of piles and pile groups in layered soil media. Soil Dyn Earthq Eng 1991;10(8):386–401.
[7] Dezi F, Carbonari S, Morici M. A numerical model for the dynamic analysis of inclined pile groups. Earthq Eng Struct Dyn 2016;45(1):45–68.
[8] Bordón JDR, Álamo GM, Padrón LA, Aznárez JJ, Maeso O. MultiFEBE: A multi-domain finite element–boundary element solver for linear mixed-dimensional mechanical problems. SoftwareX 2022;20:101265.
[9] Kaynia AM, Pedersen DM, Askheim H, Romero-Sánchez C. Implementation of seismic soil-structure interaction in openfast and application to an offshore wind turbine on jacket structure. Mar Struct 2025;103:103832.
[10] Medina C, Aznárez JJ, Padrón LA, Maeso O. Effects of soil–structure interaction on the dynamic properties and seismic response of piled structures. Soil Dyn Earthq Eng 2013;53:160–75.
[11] Mylonakis G, Nikolaou A, Gazetas G. Soil–pile–bridge seismic interaction: kinematic and inertial effects. Part I: soft soil. Earthq Eng Struct Dyn 1997;26(3):337–59.
[12] Carbonari S, Dezi F, Leoni G. Seismic soil–structure interaction in multi-span bridges: application to a railway bridge. Earthq Eng Struct Dyn 2011;40(11):1219–39.
[13] González F, Carbonari S, Padrón LA, Morici M, Aznárez JJ, Dezi F, Maeso O, Leoni G. Benefits of inclined pile foundations in earthquake resistant design of bridges. Eng Struct 2020;203:109873.
[14] González F, Padrón LA, Carbonari S, Morici M, Aznárez JJ, Dezi F, Leoni G. Seismic response of bridge piers on pile groups for different soil damping models and lumped parameter representations of the foundation. Earthq Eng Struct Dyn 2019;48(3):306–27.
[15] Álamo GM, Bordón JDR, Aznárez JJ, Maeso O. Relevance of soil-pile tangential tractions for the estimation of kinematic seismic forces: Formulation and setting of a Winkler approach. Appl Math Model 2018;59:1–19.
[16] Makris N, Gazetas G. Dynamic pile-soil-pile interaction. Part II: Lateral and seismic response. Earthq Eng Struct Dyn 1992;21(2):145–62.
[17] Matlock H. Correlation for design of laterally loaded piles in soft clay. In: Offshore technology conference. OTC; 1970, p. OTC–1204.
[18] (API) API. Recommended practice for planning, designing, and constructing fixed offshore platforms—Working stress design. 22th ed.. Washington, D.C.: American Petroleum Institute; 2014.
[19] Di Laora R, Rovithis E. Design of piles under seismic loading. In: Analysis of pile foundations subject to static and dynamic loading. CRC Press; 2021, p. 269–300.
[20] Kavvads M, Gazetas G. Kinematic seismic response and bending of free-head piles in layered soil. Geotechnique 1993;43(2):207–22.
[21] Dezi F, Carbonari S, Leoni G. Kinematic bending moments in pile foundations. Soil Dyn Earthq Eng 2010;30(3):119–32.
[22] Di Laora R, Mylonakis G, Mandolini A. Pile-head kinematic bending in layered soil. Earthq Eng Struct Dyn 2013;42(3):319–37.
[23] Dezi F, Carbonari S, Leoni G. A model for the 3D kinematic interaction analysis of pile groups in layered soils. Earthq Eng Struct Dyn 2009;38(11):1281–305.
[24] Anoyatis G, Lemnitzer A. Kinematic Winkler modulus for laterally-loaded piles. Soils Found 2017;57(3):453–71.
[25] Anoyatis G, Di Laora R, Mandolini A, Mylonakis G. Kinematic response of single piles for different boundary conditions: analytical solutions and normalization schemes. Soil Dyn Earthq Eng 2013;44:183–95.
[26] Fan K, Gazetas G, Kaynia A, Kausel E, Ahmad S. Kinematic seismic response of single piles and pile groups. J Geotech Eng 1991;117(12):1860–79.
[27] Stacul S, Rovithis E, Di Laora R. Kinematic soil–pile interaction under earthquake-induced nonlinear soil and pile behavior: An equivalent-linear approach. J Geotech Geoenvironmental Eng 2022;148(7):04022055.
[28] Di Laora R, Rovithis E. Kinematic bending of fixed-head piles in nonhomogeneous soil. J Geotech Geoenvironmental Eng 2015;141(4):04014126.
[29] Hashash YM, Park D. Non-linear one-dimensional seismic ground motion propagation in the mississippi embayment. Eng Geol 2001;62(1–3):185–206.
[30] Kondner RL. A hyperbolic stress-strain formulation for sands. In: Proc. 2nd pan-American conf. on SMFE. vol. 1, 1963, p. 289–324.
[31] Matasović N, Vucetic M. Cyclic characterization of liquefiable sands. J Geotech Eng 1993;119(11):1805–22.
[32] Gazetas G, Dobry R. Simple radiation damping model for piles and footings. J Eng Mech 1984;110(6):937–56.
[33] Chopra AK. Dynamics of structures: theory and applications to earthquake engineering. 4th ed.. Prentice-Hall International Series in Civil Engineering and Engineering Mechanics; 2011.
[34] Kramer SL. Geotechnical earthquake engineering. Upper Saddle River, NJ: Prentice Hall; 1996.
[35] Kwok AO, Stewart JP, Hashash YM, Matasovic N, Pyke R, Wang Z, Yang Z. Use of exact solutions of wave propagation problems to guide implementation of nonlinear seismic ground response analysis procedures. J Geotechnical Geoenvironmental Eng. 2007;133(11):1385–98.
[36] Hashash YM, Park D. Viscous damping formulation and high frequency motion propagation in non-linear site response analysis. Soil Dyn Earthq Eng 2002;22(7):611–24.
[37] Board of Trustees of University of Illinois at Urbana-Champaign. DEEPSOIL (2024, V7.1), a nonlinear and equivalent linear seismic site response of 1-D soil columns, user manual. 2024, Urbana, IL.
[38] Di Laora R, Mylonakis G, Mandolini A. Size limitations for piles in seismic regions. Earthq Spectra 2017;33(2):729–56.

[39] Gazetas G, Dobry R. Horizontal response of piles in layered soils. J Geotech Eng 1984;110(1):20–40.

[40] AASHTO. AASHTO LRFD bridge design specifications (10th Edition, 2024). 10th ed.. American Association of State Highway and Transportation Officials; 2025.

[41] Darendeli MB. Development of a new family of normalized modulus reduction and material damping curves. The university of Texas at Austin; 2001.

[42] Vucetic M, Dobry R. Effect of soil plasticity on cyclic response. J Geotech Eng 1991;117(1):89–107.

[43] Casablanca O. Periodic foundation piles for the seismic protection of structures. Soil Dyn Earthq Eng 2024;182:108742.

[44] Dobry R, Whitman RV, Vinuesa JMR. Soil properties and the one-dimensional theory of earthquake amplification. MIT Department of Civil Engineering, Inter-American Program; 1971.

[45] Rovithis E, Parashakis H, Mylonakis G. 1D harmonic response of layered inhomogeneous soil: Analytical investigation. Soil Dyn Earthq Eng 2011;31(7):879–90.

[46] Peng X-B, Ren W-J, Li T-Q, Xue Y-Y, Tao X-S, Xu L-Y. Seismic response of deep soft soil sites with varying shear wave velocities. Front Earth Sci 2024;12:1488519.

[47] Travasarou T, Gazetas G. On the linear seismic response of soils with modulus varying as a power of depth: the maliakos marine clay. Soils Found 2004;44(5):85–93.

[48] Pacific Earthquake Engineering Research Center (PEER)2022. NGA-West2 Ground Motion Database. 2022, [Accessed 20 August 2022], Available online: https://ngawest2.berkeley.edu/.